bioRxiv preprint doi: https://doi.org/10.1101/609735; this version posted April 15, 2019. The copyright holder for this preprint (which was not certified by peer review) is the author/funder. All rights reserved. No reuse allowed without permission.

Amelioration of muscular dystrophy phenotype in mdx mice by inhibition of Flt1

Mayank Verma[a,b,c,d], Yuko Shimizu-Motohashi [b,c,d], Yoko Asakura [b,c,d], James Ennen[b,c,d], Jennifer Bosco[f], Zhiwei Zou[f], Guo-Hua Fong[e], Serene Josiah[f], Dennis Keefe[f] and Atsushi Asakura[b,c,d,g]

[a]Medical Scientist Training Program, [b]Stem Cell Institute, [c]Paul & Sheila Wellstone Muscular Dystrophy Center, [d]Department of Neurology, University of Minnesota Medical School. Minneapolis, MN, USA, [e]Center for Vascular Biology, University of Connecticut Health Center, University of Connecticut School of Medicine, Farmington, CT, USA, [f]Shire Human Genetic Therapies(HGT), Lexington, MA, USA, a member of the Takeda group of companies..

[g]**Corresponding Author:** Atsushi Asakura (asakura@umn.edu)

bioRxiv preprint doi: https://doi.org/10.1101/609735; this version posted April 15, 2019. The copyright holder for this preprint (which was not certified by peer review) is the author/funder. All rights reserved. No reuse allowed without permission.

Abstract

Duchenne muscular dystrophy (DMD) is an X-linked recessive genetic disease in which the dystrophin coding for a membrane stabilizing protein is mutated. Recently, the vasculature has also shown to be perturbed in DMD and DMD model *mdx* mice. Data-mining DMD transcriptomics revealed the defects were correlated to a vascular endothelial growth factor (VEGF) signaling pathway. To reveal the relationship between DMD and VEGF signaling, *mdx* mice were crossed with constitutive ($CAG^{/CreERTM}$:$Flt1^{LoxP/LoxP}$) and endothelial cell-specific conditional gene knockout mice ($Cdh5^{CreERT2}$:$Flt1^{LoxP/LoxP}$) for *Flt1* which is a decoy receptor for VEGF. Previous work demonstrated that heterozygous global *Flt1* knockout mice increased vascular density and improved DMD phenotypes when crossed with DMD model *mdx* and *mdx:utrn*$^{-/-}$ mice. Here, we showed that while constitutive deletion of *Flt1* is detrimental to the skeletal muscle function, endothelial cell-specific *Flt1* deletion resulted in increased vascular density and improvement in the DMD-associated phenotype in the *mdx* mice. These decreases in pathology, including improved muscle histology and function, were recapitulated in *mdx* mice given anti-FLT1 peptides or monoclonal antibodies, which blocked VEGF-FLT1 binding. The histological and functional improvement of dystrophic muscle by FLT1 blockade provides a novel pharmacological strategy for the potential treatment of DMD.

bioRxiv preprint doi: https://doi.org/10.1101/609735; this version posted April 15, 2019. The copyright holder for this preprint (which was not certified by peer review) is the author/funder. All rights reserved. No reuse allowed without permission.

Introduction

Duchenne Muscular Dystrophy (DMD) is an X-linked muscle disease affecting one in 5,000 new born males, in which the gene encoding the dystrophin protein is mutated. It is a progressive neurodegenerative disease with clinical symptoms manifesting at 2-3 years of age, loss of ambulation in early teen years and death by either respiratory insufficiency or cardiac failure in their 20s. A disease model for DMD is the *mdx* mouse, which lacks functional dystrophin expression due to a point mutation in the dystrophin gene. The mdx mouse has and been extensively characterized and contributed to the understanding of the disease pathology (2).

Although the role of dystrophin in the skeletal muscle is widely appreciated, endothelium and vascular smooth muscle also express dystrophin (3). The absence of dystrophin in these cells resulted in vessel dilation and abnormal blood flow, resulting in a state of functional ischemia, worsening the muscle pathology in *mdx* mice (4). Restoration of dystrophin specifically in the smooth muscle of the vasculature rescued improved some aspects of the skeletal muscle pathology associated with the *mdx* mice (5). Disruption of the dystrophin-associated sarcoglycan complex in vascular smooth muscle perturbed vascular function resulting in exacerbation of skeletal muscler dystrophic changes (6). Dystrophin is responsible for linking neuronal nitric oxide synthase (nNOS) to the cell surface, which is crucial for exercise-induced increases in blood supply in muscle via NO-mediated vasodilation (7). Administration of a phosphodiesterase-5 (PDE-5) inhibitors to *mdx* mice, which increased NO production, rescued the muscle from this state of functional ischemia, and resulted in improved muscle function in mdx mice (8, 9). Similarly in humans, PDE-5 inhibitors given to both adult patients with Becker muscular dystrophy, a milder form of muscular dystrophy, and DMD boys, alleviated functional ischemia during muscle contraction (10, 11). More recent data showes that *mdx* skeletal muscle

bioRxiv preprint doi: https://doi.org/10.1101/609735; this version posted April 15, 2019. The copyright holder for this preprint (which was not certified by peer review) is the author/funder. All rights reserved. No reuse allowed without permission.

was less perfused and displayed marked microvessel alterations compared to control *C57BL6* mice (12, 13). While current studies support the importance of NO-mediated vasodilation in DMD, the relationship between DMD and angiogenesis is not well understood.

Vascular endothelial growth factor (VEGF) signaling is one of the strongest modulators of angiogenesis and includes the ligands VEGFA, VEGFB, VEGFC and PDGF. VEGFA is the most well studied ligand of the system and acts through its two receptors, VEGF receptor-1 (VEGFR1/FLT1) and VEGF receptor-2 (VEGFR2/ FLK1/KDR). Although FLK1 possesses stronger signaling capabilities, FLT1 has considerable higher affinity for VEGF but weaker signaling capabilities . In normal tissue, FLT1 acts as a sink trap for VEGF thereby preventing excessive pathological angiogenesis. In addition, soluble FLT1 (sFLT1) functions as an endogenous VEGF trap (14). Despite the known angiogenic defect in DMD and *mdx* mice, it is not known whether VEGF and its receptors are implicated in this disease process. Previous data from our laboratory demonstrated that heterozygous *Flt1* gene knockout mice were viable and displayed developmentally increased capillary density in the skeletal muscles examined (1). Importantly, when crossed with *mdx* or *mdx/utrn*$^{-/-}$ double knockout mice, these mice displayed both histological and functional improvements of the dystrophic pathologic phenotype. However, it remained unknown whether postnatal *Flt1* gene deletion and pharmacological blockage of Flt1 could recapitulate these improvements in *mdx* mice.

In this report, we compared adult mdx mice with either a constitutive conditional knockout or an endothelial cell-specific conditional knockout of *Flt1*. We showed that endothelial cell-specific *Flt1* deletion increased the capillary density in skeletal muscle and improved the DMD-associated muscle pathology. In addition, we showed that intravenous administration of anti-FLT1 peptides and monoclonal antibodies (MAbs) in *mdx* mice

bioRxiv preprint doi: https://doi.org/10.1101/609735; this version posted April 15, 2019. The copyright holder for this preprint (which was not certified by peer review) is the author/funder. All rights reserved. No reuse allowed without permission.

recapitulated the reduction in DMD-associated pathology seen after *Flt1* deletion in *mdx* mice, validating *Flt1* as a therapeutic target for the treatment of DMD.

bioRxiv preprint doi: https://doi.org/10.1101/609735; this version posted April 15, 2019. The copyright holder for this preprint (which was not certified by peer review) is the author/funder. All rights reserved. No reuse allowed without permission.

Results

Postnatal *Flt1* gene deletion in mice display increase in capillary density

We previously found that *mdx* mice developmentally lacking one copy of the *Flt1* allele have increased muscle angiogenesis and improved muscle pathology[13]. To investigate whether postnatal deletion of *Flt1* gene could affect the vasculature density, we crossed $CAG^{CreERTM}$ mice carrying a constitutively expressed $CreER^{TM}$ gene (15) with $Flt1^{LoxP/LoxP}$ mice (16) to generate conditional $Flt1^{\Delta/\Delta}$ ($Flt1^{LoxP/LoxP}$: $CAG^{CreERTM}$) mice (Figure 1A). Upon treatment with tamoxifen (TMX), which leads to global *Flt1* gene and FLT1 protein deletion (Supplemental Figure 1A, B), $Flt1^{\Delta/\Delta}$ mice displayed significantly increased CD31+ vascular density compared to the $Flt1^{+/+}$ ($CAG^{CreERTM}$:$Flt1^{LoxP/LoxP}$) mice (Figure 1B, C). The increase in capillary density following TMX-mediated *Flt1* gene deletion was rapid (within 8 days) and long lasting (more than 207 days) (Figure D). This allowed us to be confident that we were able to phenotype late term changes following deletion of *Flt1* gene. Postnatal global loss of *Flt1* resulted in a reduction in body mass without reduction of tibialis anterior (TA) muscle mass (Supplemental Figure 1C, D, E) (17).

mdx:Flt1$^{\Delta/\Delta}$ mice display worse muscle pathology compared to control *mdx:Flt1*$^{+/+}$ mice

As we did not see any gross changes in the skeletal muscle except for increased vascular density in the $Flt1^{\Delta/\Delta}$ mice, we crossed the *mdx* mice to the $Flt1^{\Delta/\Delta}$ to obtain *mdx*:$Flt1^{\Delta/\Delta}$ mice. We obtained the mice in expected mendelian ratios (Supplemental Figure 2A). Our original goal was to induce *Flt1* gene deletion prior to the onset of muscle pathology, thus before postnatal day 21 (p21), by treatment with TMX or its active form, 4-hydroxy tamoxifen (4-OHT). However, perinatal loss of *Flt1* resulted in lethality when TMX or 4-OHT treatment was initiated at p3 or

bioRxiv preprint doi: https://doi.org/10.1101/609735; this version posted April 15, 2019. The copyright holder for this preprint (which was not certified by peer review) is the author/funder. All rights reserved. No reuse allowed without permission.

p5 and partial lethality at p16 (Supplemental Figure 2B), indicating that *Flt1* is required in the perinatal stage for survival. The mice displayed no lethality when recombination was induced on or after p21. Importantly, the increase in capillary density by loss of the *Flt1* gene was maintained in the *mdx* background in the *mdx:Flt1*$^{\Delta/\Delta}$ mice (Figure 2A). This was accompanied by a physiological increase in skeletal muscle perfusion as shown by laser Doppler imaging (Figure 2B). The *mdx:Flt1*$^{\Delta/\Delta}$ mice showed a shift in fiber type composition toward increases in oxidative type I fibers (Supplemental Figure 3A, B). This was more pronounced in the EDL compared to the soleus, which is already predominantly type I.

Next, we proceeded to look for dystrophinopathy-related muscle changes in the adult *mdx:Flt1*$^{\Delta/\Delta}$ mice. Similar to the *Flt1*$^{\Delta/\Delta}$ mice, body mass decreased without changing muscle mass in *mdx:Flt1*$^{\Delta/\Delta}$ mice compared with *mdx:Flt1*$^{+/+}$ mice (Supplemental Figure 3C, D). The *mdx:Flt1*$^{\Delta/\Delta}$ mice displayed notable white fur, a sign of premature aging or stress (Supplemental Figure 3E). Evans blue dye (EBD) accumulation (21) showed no differences, while fibrosis was markedly increased in the *mdx:Flt1*$^{\Delta/\Delta}$ mice (Figure 2 C, D, E). Embryonic MHC (eMHC)+ muscle fibers increased in the *mdx:Flt1*$^{\Delta/\Delta}$ mice (Supplemental Figure 3F), suggesting increased myofiber regeneration. There is no improvement in grip strength generation by the mice (Figure 2F). Taken together, the *mdx:Flt1*$^{\Delta/\Delta}$ mice showed an increase in capillary density but increased muscle pathology.

Endothelial cell-specific loss of *Flt1* in *mdx* improves muscle phenotype in *mdx* mice.

Flt1 is expressed in several cell types including endothelial cells, myeloid cells and some neurons. Thus, we hypothesized that *Flt1* may be indispensable in one of these other compartments. Since endothelial cell-specific *Flt1* deletion resulted in increased capillary density

bioRxiv preprint doi: https://doi.org/10.1101/609735; this version posted April 15, 2019. The copyright holder for this preprint (which was not certified by peer review) is the author/funder. All rights reserved. No reuse allowed without permission.

in heart and adipose tissue (16, 22), we hypothesized that deletion of endothelial cell-specific *Flt1* would be sufficient to increase angiogenesis and improve muscle pathology in the *mdx* mice.

We attempted to increased the angiogenesis in skeletal muscle using an endothelial cell-specific *VE-cadherin (Cdh5)-CreERT2*-mediated *Flt1* deletion in mice. *Cdh5* is an endothelial cell-specific cadherin gene used for lineage tracing and conditional deletion of endothelial cells (23). Goel. et al. recently reported the presence of Cdh5 in satellite cells questioning the validity of using $Cdh5^{Cre\text{-}ERT2}$ in skeletal muscle tissue (24). We verified the endothelial cell specificity of the $Rosa26R^{mTmG}$ reporter, and Cre-mediated excision resulted in the mGFP expression in the endothelial cells but no other cell types (Supplemental Figure 4A, B, C). We confirmed that the $Cdh5^{CreERT2}$ was not present in the Pax7+ satellite cells using single muscle fiber immunostaining (data not shown). We saw no difference in the body mass or muscle mass in endothelial cell-specific *Flt1* deleted mice compared with the control mice (Supplemental Figure 4D, E).

We crossed the *mdx:*$Flt1^{LoxP/LoxP}$ mice to the $Cdh5^{CreERT2}$ mice to yield the *mdx:Cdh5-*$Flt1^{\Delta/\Delta}$ mice (Figure 3A). Upon TMX treatment, capillary density and laser Doppler flow increased in the skeletal muscle in *mdx:Cdh5-*$Flt1^{\Delta/\Delta}$ mice compared with *mdx:Cdh5-*$Flt1^{+/+}$ *mdx:Cdh5-*$Flt1^{+/\Delta}$ mice, indicating that endothelial cell-specific deletion of *Flt1* was sufficient to increase capillary density in the skeletal muscle (Figure 3B, C). This was accompanied by a physiological increase in skeletal muscle perfusion using laser Doppler (Figure 3D). Moreover, the *mdx:Cdh5-*$Flt1^{\Delta/\Delta}$ did not show any significant changes in body and muscle mass loss (Supplemental Figure 5). Signs of DMD-associated pathology such as increased EBD uptake and fibrosis were significantly reduced in the *mdx:Cdh5-*$Flt1^{\Delta/\Delta}$ mice (Figures 3B, E, F). The muscle fibers the *mdx:Cdh5-*$Flt1^{\Delta/\Delta}$ mice had decreased centrally located nuclei and maintained larger myofibers fibers compared with the *mdx:Cdh5-*$Flt1^{+/+}$ mice (Figure 4A, B, C). The histological

bioRxiv preprint doi: https://doi.org/10.1101/609735; this version posted April 15, 2019. The copyright holder for this preprint (which was not certified by peer review) is the author/funder. All rights reserved. No reuse allowed without permission.

improvements correlated with a functional improvementas the *mdx:Cdh5-Flt1*$^{\Delta/\Delta}$ mice showed increased grip strength compared with the *mdx:Cdh5-Flt1*$^{+/+}$ mice (Figure 4D). Taken together, these data indicate that endothelial cell-specific *Flt1* loss was sufficient to increase capillary density and decreases muscle pathology in the *mdx* mice.

Pharmacological inhibition of FLT1 improved *mdx* mice.

The genetic model of *Flt1* deletion showed an ameliorated phenotype in the *mdx* mice. To translate our genetic results into therapeutic approaches for DMD model mice, we utilized a previously reported anti-FLT1 hexapeptide (Gly-Asn-Gln-Trp-Phe-Ile or GNQWFI) that inhibits VEGF-binding to FLT1. Intramuscular administration of the anti-FLT1 peptide in TA muscle of perinatal *mdx* mice (Supplemental Figure 6A) increased capillary density and decreased muscle pathology in the treated muscle (Supplemental Figure 6B-D). We assessed the diaphragm muscle after systemic (IP) injection of the anti-Flt1 peptide at a low (10 mg/kg body weight) and a high dose (100 mg/kg body weight) to test for therapeutic potential (Figure 5A). While treatment with a low dose of anti-FLT1 peptide had no effect on capillary density, membrane permeability, or fibrosis, the high dose increased capillary density (Figure 5B and C), decreased EBD+ fibers (Figure 5B, D), and decreased fibrosis (Figure 5B, E). Anti-FLT1 peptide-treated *mdx* mice showed increased skeletal muscle perfusion using laser Doppler and generated increased grip strength compared with the *mdx* mice (Figure 5F, G). There was no significant body mass alteration following anti-FLT1 peptide treatment (Supplemental Figure 6E, F). To increase stability and the hydrophobicity (25), we tested a D-isoform anti-FLT1 peptide attached to polyethylene glycol (PEG). However, systemic administration of the PEG-D-form anti-FLT1 peptide did not increase capillary density or improve muscle pathology or function in the *mdx*

bioRxiv preprint doi: https://doi.org/10.1101/609735; this version posted April 15, 2019. The copyright holder for this preprint (which was not certified by peer review) is the author/funder. All rights reserved. No reuse allowed without permission.

mice (Supplemental Figure 7). Taken together, these proof-of-concept experiments showed that postnatal inhibition of FLT1 by anti-FLT1 peptide could ameliorate the pathology associated with DMD in the *mdx* mice. However, the functional dose (100 mg/kg body weight) was orders of magnitude higher than the generally acceptable pharmacological standards of body weight dosage for small molecule drugs (26). A more potent or alternative strategy is required for further translational studies.

Screening for antibody against FLT1

As postnatal gene deletion and pharmacological inhibition of FLT1 decreased the muscular dystrophy-associated pathology in the *mdx* mice, we next sought to examine whether it could do this in a more translational manner using biologics to block FLT1. To establish proof of principle, we screened 8 commercially available MAbs that could block VEGFA-FLT1 binding. We first screened for the ability of the MAbs to block chimeric FLT1-FC binding to PLGF2, a VEGF family protein, using ELISA (Supplemental Figure 8A, B), since both PLGF2 and VEGFA occupy the same binding sites on the extracellular domain of FLT1 (27). Three MAbs showed higher binding affinities; EWC (from Novus), MAB0702 Mab (from Angio-Proteomie), and EWC (from Acris) blocked binding by 65.4%, 64.8%, and 60.6%, respectively, while the control polyclonal anti-FLT1 antibody could block 83.1% of binding (Supplemental Figure 8B). We selected two MAbs (MAB0702 and EWC) for further analyses based on their blocking efficiency and their availability for large *in vivo* studies. The MAB0702 and EWC were raised against the extracellular domains of the human FLT1, respectively, and likely target both membrane-bound (mFLT1) and sFLT1 due to similar homology of epitopes. We validated the blocking affinity to FLT1-VEGFA binding, and found that MAB0702 and EWC blocked binding by 40.1% and

bioRxiv preprint doi: https://doi.org/10.1101/609735; this version posted April 15, 2019. The copyright holder for this preprint (which was not certified by peer review) is the author/funder. All rights reserved. No reuse allowed without permission.

19.9%, respectively, compared to the 94.3% for the polyclonal control (Supplemental Figure 8C). We further determined the antibodies' affinities against mouse and human FLT1-FC protein using Biacore analysis (Supplemental Table 1). MAB0702 and EWC had similar association rate/binding constants for both mouse and human FLT1-FC. By contrast, MAB0702 had significantly higher dissociation constants for mouse FLT1-FC compared with EWC, while MAB0702 had lower dissociation constants for human FLT1-FC compared with EWC. Based on these affinity studies, we decided to utilize both MAB0702 and EWC MAbs for *in vivo* experiments.

Testing Anti-FLT1 antibody treatment for DMD

We IV injected MAB0702 at a dose of 20 mg/kg body weight into *mdx* mice, and measured free sFLT1 and VEGFA in the serum. We found a significant decrease in free serum sFLT1 (Supplemental Figure 8C) and an increase in serum VEGFA levels (Supplemental Figure 8D) following MAB0702 injection, suggesting the efficient blocking of MAB0702 to sFLT1 and FLT1 *in vivo*. Based on our screening results, we performed experiments according to the experimental schema (Figure 6A). *mdx* mice were injected with IV MAbs or isotype control IgG dosing at 2 mg/kg or 20 mg/kg body weight every 3 days for four weeks beginning at 3 weeks of age (Figure 6A). While capillary density was not altered by treatment with either MAB0702 or EWC at 2 mg/kg body weight (data not shown), the treatment with MAB0702 at 20 mg/kg body weight but not EWC or isotype control significantly increased capillary density (Figure 6B, C). More importantly, the mice treated with MAB0702 at 20 mg/kg body weight also displayed improved histology, such as decreased number of EBD+ fibers, decreased fibrosis, decreased calcification, and decreases in CLN (Figures 6B, D, E, F, G, 7A, B) without affecting any body

bioRxiv preprint doi: https://doi.org/10.1101/609735; this version posted April 15, 2019. The copyright holder for this preprint (which was not certified by peer review) is the author/funder. All rights reserved. No reuse allowed without permission.

weight compared with the *mdx* mice (Supplemental Figure 8E, F). Treatment prevented the increase in smaller caliber myofibers seen in the mdx mice (Figure 7A, C). While the EWC had significantly lower dissociation constants to mouse FLT1 compared with MAB0702 (Supplemental Table 1), we were surprised to find that *in vivo* administration of the EWC did not induce changes in capillary density or muscle pathology (Figures 6B, C, D, E, F, G, 7A, B). MAB0702-treated *mdx* mice generated increased grip strength compared with the *mdx* mice (Figure 7D). Skeletal muscle endurance, as assessed by treadmill running as an indicator of maximal muscle capacity, showed running duration and distance of MAB0702-treated *mdx* mice significantly increased compared to *mdx* mice (Figure 7E, F). Thus, anti-FLT1 antibody administration depleted free serum FLT1 levels and increased free serum VEGFA levels, which led to increased angiogenesis and reduced muscle pathology in *mdx* mice, providing a potential new pharmacological strategy for treatment of DMD.

VEGFA signaling is perturbed in DMD animal models and DMD patients.

While angiogenic defects have been reported in the *mdx* mice, it is not known whether VEGF family and its downstream targets are implicated in dystrophinopathies. We probed the VEGF ligands and receptors in microarrays from skeletal muscles from *mdx* mice and the golden retriever muscular dystrophy (GRMD) canine model of DMD. *VEGFA* was downregulated in both models (Figure 8A). *Flt1* was downregulated in GRMD but not *mdx* muscles. To examine whether VEGF signaling is altered in DMD patients, we performed gene expression analysis on previously available data from microarrays and RNA-seq from patients with DMD. We also aggregated and probed microarrays data from muscle biopsies of patients with numerous neuromuscular diseases or after exercise. In the microarray data, *VEGFA* expression was

bioRxiv preprint doi: https://doi.org/10.1101/609735; this version posted April 15, 2019. The copyright holder for this preprint (which was not certified by peer review) is the author/funder. All rights reserved. No reuse allowed without permission.

increased after an acute bout of exercise, and VEGFA expression was reduced in ALS muscle, BMD muscle, as well as both early and late phases of DMD muscle (28) (Figure 8B). This was corroborated by RNAseq data (Figure 8C). Angiogenic genes downstream of VEGF, such *HRAS*, *KRAS* and *NRAS,* were downregulated in DMD and BMD muscle despite an increase in VEGF pathways such as *HIF1A* (Figure 8D). By contrast, the expression of VEGF receptors (*Flt1* and *Flk1*) and the coreceptors (*Nrp1* and *Nrp2*) was not significantly changed in DMD muscle (Figure 8B, C). These data indicate that VEGFA expression is decreased in dystrophinopathy, and thus may benefit people with DMD by either increasing VEGFA and/or decreasing sFLT1 as a therapeutic target.

Discussion

In this report, we show that *Flt1* is important postnatally as conditional *Flt1* deletion in *mdx:Flt1*$^{\Delta/\Delta}$ mice in the perinatal stage results in lethality in mice. While deletion of *Flt1* in neonates increased capillary density in both C57Bl6 and *mdx* mice, it leds to the worsening of the skeletal muscle phenotype. *Flt1* is expressed in several cell types including endothelial cells, myeloid cells and some neurons (23, 29–31). Thus, *Flt1* may be indispensable in one of these other compartments when perinatally deleted. For example, *Flt1* is expressed in motor neurons, where is not simply acting as a VEGFA sink-trap, but its tyrosine kinase activity it is responsible for motor neuron survival (29). Thus, increased angiogenesis but worse pathological alterations in *mdx:Flt1*$^{\Delta/\Delta}$ muscle may be due to motor neuron–associated changes. By contrast, loss of *Flt1* in endothelial cells in the postnatal stage increased the capillary density and blood perfusion in skeletal muscle without significant decreases in weight or muscle mass. Increased angiogenesis and blood perfusion were observed in the global *Flt1* heterozygous knockout mice (1), indicating that loss of endothelial cell-specific *Flt1* in *mdx:Cdh5-Flt1*$^{\Delta/\Delta}$ mice was sufficient to produce

bioRxiv preprint doi: https://doi.org/10.1101/609735; this version posted April 15, 2019. The copyright holder for this preprint (which was not certified by peer review) is the author/funder. All rights reserved. No reuse allowed without permission.

increased capillary density and vascular perfusion in the skeletal muscle. This also led to an decrease in *mdx*-associate mucle pathology, confirming that postnatal deletion of *Flt1* is able to rescue the dystrophinopathy related muscle pathology.

Importantly, for the first time, we demonstrated that administration of both anti-FLT1 peptide and anti-FLT1 MAb increased angiogenesis, which leds to an decrease in the pathology associated with DMD in *mdx* mice and is a phenocopy of our genetic models (*mdx:Cdh5-Flt1*$^{\Delta/\Delta}$ mice). We screened commercially available MAbs for blocking ligands-FLT1 and ligands-sFLT1, and demonstrated that administration of MAB0702 MAbs was able to phenocopy our genetic model in a manner suited for translational studies to reduce muscle pathology in *mdx* mice. Improvement of dystrophic muscle function by FLT1 blockade may provide a novel pharmacological strategy for treatment of diseases associated with DMD via increased serum and tissue VEGFA levels, which induce increased vascular density and blood perfusion.

After MAB0702 administration, we showed a small increase in VEGFA levels in serum. It should be noted that a mere 2-fold increase of VEGFA during development is incompatible with life in transgenic mice (32). Computation and experimental models showed that local VEGF gradients are more important than the total concentration (33–36). We recently demonstrated that muscle satellite cells express abundant VEGFA, which recruits endothelial cells and capillaries to the proximity of satellite cells on muscle fibers (37). Taken together, these data strongly suggest that hot-spots with high levels of VEGFA in *Flt1* knockout or anti-FLT1 treated mice may result in increased capillary density and vascular perfusion, which is predicted to result in decreased associated DMD-type pathological changes in the skeletal muscles.

While VEGFA binds to both FLT1 and FLK1, VEGFB, PlGF1and PlGF2 only bind to FLT1 (38). This creates a scenario where PlGF1/2 and VEGFB binding can sequester FLT1,

bioRxiv preprint doi: https://doi.org/10.1101/609735; this version posted April 15, 2019. The copyright holder for this preprint (which was not certified by peer review) is the author/funder. All rights reserved. No reuse allowed without permission.

increasing serum and tissue VEGFA availability for VEGFA-FLK1 binding-mediated angiogenic induction. While *PlGF* is dispensable for normal development and health and not expressed in the normal adult tissues outside the female reproductive organs (39), VEGFB is expressed in the muscle tissue and muscle fibers (40). VEGFB may play a role in diet induced obesity and free fatty uptake by the endothelial cells in skeletal muscle (41), but this remains controversial (22). However, VEGFB overexpression does not result in an angiogenic response in ischemic skeletal muscle (42), indicating that blocking VEGFB-FLT1 signaling is not likely to be responsible for the angiogenic changes seen in this study.

The present study shows that increased angiogenesis may be a novel avenue to improve some of pathology associated with loss of dystrophin, including function, and could be used in conjunction with other treatment strategies. For example, intramuscular injection of VEGF containing recombinant adeno-associated viral vectors resulted in both functional and histological improvements in both ischemic and *mdx* muscle (19, 49, 50). This improvement was seen in combination with increased in angiogenesis in the muscle. Increased capillary density in the *mdx* muscle work through paracrine stimulation, by protecting muscle fiber damage and promoting satellite cell proliferation, survival and self-renewal in the vascular niche (37, 43). Christov et al. and our group showed that satellite cells were preferentially located next to capillaries (37, 44). Since our approaches increased the number of capillaries found in the examined muscles, it may effectively increase the amount of vascular niche that houses the satellite cell compartment in the muscle. Recently, we showed that genes encoding for endothelial and satellite cells were highly correlated across muscle groups, and endothelial cells could mediate satellite cell self-renewal via Notch activation (37) .Therefore, increase in the vascular niche may increase satellite cell self-renewal and the number of myogenic precursor

bioRxiv preprint doi: https://doi.org/10.1101/609735; this version posted April 15, 2019. The copyright holder for this preprint (which was not certified by peer review) is the author/funder. All rights reserved. No reuse allowed without permission.

cells, which we hypothesize may be responsible for the improved phenotype seen in the *mdx* mice with *Flt1* deletion or functional blockage.

MAb-based therapeutics for the treatment of DMD have been developed to increase muscle mass via targeting myostatin and to decrease fibrosis via targeting fibroadipogenic progenitors (45). Further optimization using with humanized antibodies are required for future translation to humans (46). Taken together, we have gathered evidence for the first time that FLT1-targeted MAbs may be an effective therapeutic approach for the treatment of DMD.

bioRxiv preprint doi: https://doi.org/10.1101/609735; this version posted April 15, 2019. The copyright holder for this preprint (which was not certified by peer review) is the author/funder. All rights reserved. No reuse allowed without permission.

Methods

Mice

Flt1$^{Loxp/Loxp}$ were obtained from Dr. Gua-Hua Fong (16). *Cdh5*^{CreER} mice were obtained from Dr. Yoshiaki Kubota (23). B6Ros.Cg-*Dmd*$^{mdx\text{-}5Cv}$/J (*mdx*; JAX stock #002379)(47), B6.Cg-Tg(CAG-cre/Esr1*)5Amc/J (*CAG*^{CreERTM}; JAX stock #004682)(15). D2.129(Cg)-*Gt(ROSA)26Sor*$^{tm4(ACTB\text{-}tdTomato,\text{-}EGFP)Luo}$/J (mT/mG- JAX stock #007576)(48) were obtained from Jackson Laboratory. Colonies for all the mice were established in the laboratory. Cre recombination was induced using tamoxifen (TMX) (Sigma-Aldrich, T5648) dosed as 75 mg/kg body weight x 3 time over one week at 3-4 weeks of age unless otherwise specified. We also injected 4-hydroxy tamoxifen (4-OHT) (Sigma-Aldrich, H6278) dosed as 25 mg/kg body weight. Control mice contained the wild-type (WT) Cre allele or were injected with the vehicle (corn oil or 10% ethanol). All animal studies were approved by the IACUC at University of Minnesota.

Anti-FLT1 peptides and antibodies

The anti-FLT1 peptide was synthesized from Peptide 2.0 Inc based on the sequence (Gly-Asn-Gln-Trp-Phe-Ile or GNQWFI) as previously described (49). DMSO was used to dissolve the peptide. Twenty μg of peptide diluted in 2% DMSO in PBS solution for intramuscular injection per day in the TA muscle. Ten mg/kg body weight and 100 mg/kg body weight were used for the systemic treatment. The second generation anti-FLT1 peptide (PEG-$G_DN_DQ_DW_DF_DI_D$) was synthesized with the following modifications: The polyethylene glycol moiety was attached to the peptide to improve solubility in polar solvents and the D isomeric form was used instead of the L to enhance stability of the peptide (25). PBS was used as a vehicle. The peptides were commercially synthesized (LifeTein, LLC). Commercially available anti-FLT1 antibodies were

bioRxiv preprint doi: https://doi.org/10.1101/609735; this version posted April 15, 2019. The copyright holder for this preprint (which was not certified by peer review) is the author/funder. All rights reserved. No reuse allowed without permission.

obtained from the manufacturer in carrier free and preservative free form. Isotype IgG (Santa Cruz Biotechnology) was used for control experiment. Two or 20 mg/kg body weight was used for the systemic treatment. Retro-orbital IV injections were performed for systemic treatment for both the peptides and the antibody treatment.

RNA and genomic DNA isolation and qPCR

Mouse TA muscle was homogenized in TRIzol™ reagent (ThermoFisher Scientific, 15596026) for RNA isolation. RNA was isolated using the Direct-zol™ RNA Microprep Kit (Zymo Research, R2062) with on-column DNase digestion followed by cDNA synthesis using the Transcriptor First Strand cDNA synthesis kit (Roche Molecular Diagnostics, 04379012001) using random primers. Genomic DNA was isolated from mouse tail snips with lysis buffer containing Protenase K (Sigma-Aldrich, P2308). Genotyping was performed by agarose gel electrophoresis-mediated detection following PCR reaction by Taq polymerase (New England Biolabs, M0273). qPCR was performed using GoTaq® *qPCR* Master Mix (Promega, A6001). Primer sequences are listed in Table S1. All primers were synthesized as custom DNA oligos from Integrated DNA technologies (IDT).

Muscle perfusion

RBC flux was evaluated using the moorLabTM laser Doppler flow meter as previously described (1). with the MP7a probe that allows for collecting light from a deeper tissue level than standard probes according to the manufacturer's instructions (Moor Instruments). The fur from the right hind leg was removed using a chemical depilatory. Readings were taken using the probe from at least 10 different spots on the TA muscle. The AU was determined as the average AU value

bioRxiv preprint doi: https://doi.org/10.1101/609735; this version posted April 15, 2019. The copyright holder for this preprint (which was not certified by peer review) is the author/funder. All rights reserved. No reuse allowed without permission.

during a plateau phase of each measurement. Microbubble angiography was performed on the Vevo 2100 (Fujifilm) with vevo micromarker contrast agent. Mice were shaved and depapilated over the medial hindlimb. Mice were sedated using 4% Isoflurane and taped to a heated platform. Pre-warmed ultrasound gel was applied to the probe and the muscle was visualized using B-mode and doppler to locate the femoral artery/vein and ROI of exact same size was drawn for the muscle around the vessels. 60ul of $2x10^9$ bubbles/ml contrast agent was administered over 2 seconds retro-orbitally and non-linear contrast imaging was performed. The peak enhancement was measured using the Vevo2100 software.

Grip strength test

Forelimb grip strength test was performed following a previously published procedure (50). Briefly, *mdx* mice were gently pulled by the tail after fore limb-grasping a metal bar attached to a force transducer (Columbus Instruments). Grip strength tests were performed by the same blinded examiner. Five consecutive grip strength tests were recorded, and then mice were returned to the cage for a resting period of 20 minutes. Then, three series of pulls were performed each followed by 20 min resting period. The average of the three highest values out of the 15 values collected was normalized to the body weight for comparison.

Treadmill running

Exer-3/6 Treadmill (Columbus Instruments) was used for treadmill running test as previously described(51). Briefly, for acclimation, mice were placed in each lane and forced to run on a treadmill for 5 minutes at a speed of 10 m/min on a 0% uphill grade for 3 days. And then, mice were forced to run on a treadmill with a 10% uphill grade starting at a speed of 10 m/min for 5

bioRxiv preprint doi: https://doi.org/10.1101/609735; this version posted April 15, 2019. The copyright holder for this preprint (which was not certified by peer review) is the author/funder. All rights reserved. No reuse allowed without permission.

minutes. Every subsequent 2 minutes, the speed was increased by 2 m/min until the mice underwent exhaustion which was defined as the inability of the mice to remain on the treadmill. The time of running as well as the distance run were recorded.

Histology and immunofluorescence

To assess the microvasculature ECs, we utilized intravital tomato-lectin (Vector labs DL-1178) staining following retro-orbital IV injections. Tissues were frozen fresh using LiN_2 chilled isopentane and stored at -80ºC. Eight μm thick transverse cryosections were used for all histological analysis. Slides were fixed using 2% PFA and washed twice using PBS + 0.01% Triton (PBST) before being used. For capillary density measurement, immunohistochemistry for CD31 was performed using anti-CD31 antibody followed by the Vectastain Elite ABC Kit (Vector Laboratories) according to the manufacturer's instructions and developed using 3-amino-9-ethylcarbazole (AEC) (Sigma-Aldrich). For immunofluorescence, sections were fixed, washed twice in PBST and blocked 5% goat serum and 0.2% Triton X-100 for 30 min. Sections were incubated with primary antibodies overnight, washed twice in PBST and incubated in fluorescent-conjugated secondary antibody for 1 hour. Anti-FLT1 (RB-9049, NeoMarkers) and anti-Laminin (4H8-2, Sigma-Aldrich) antibodies followed by anti-rabbit Alex-488 and anti-rat Alexa-568 (Molecular Probes) were used for detection of FLT1 expression in capillaries. Anti-slow MHC (NOQ7.5.4D, Sigma-Aldrich) or anti-embryonic MHC (F1.652, Developmental Study Hybridoma Bank) and anti-Laminin (4H8-2, Sigma-Aldrich) antibodies followed by anti-mouse Alex-488 and anti-rat Alexa-568 (Molecular Probes) were used for detection of slow muscle fibers. One percent Evans blue dye (EBD) (Sigma-Aldrich, E2129) dissolved in PBS were injected IP at 1% body weight 16-20 hours prior to dissecting the mouse. Sirus red, Alizarin

bioRxiv preprint doi: https://doi.org/10.1101/609735; this version posted April 15, 2019. The copyright holder for this preprint (which was not certified by peer review) is the author/funder. All rights reserved. No reuse allowed without permission.

red, and Hematoxylin & Eosin (HE) were performed as previously described (1). All sections were co-stained using DAPI and mounted using DAKO mounting media. Microscopic images were captured by a DP-1 digital camera attached to BX51 fluorescence microscope with 10x, 20× or 40× UPlanFLN objectives (all from Olympus). Fiji was used for image processing (52).

Biacore Surface Plasmon Resonance (SPR) Binding Assay for Anti-FLT1 MAbs

The single cycle kinetics method was used for sFLT1 binding assay by Biacore (GE Healthcare Bio-Science). A CM5 series S sensor chip (GE Healthcare Bio-Science) with mouse and human soluble FLT1-FC chimeric protein (R&D systems, 471-F1-100 and 321-FL-050/CF) immobilized to about 1,000 RU was used as ligand for the analyte binding of anti-FLT1 MAbs. An analyte range of 0-5 nM was used for kinetic experiments. A 5 min association step was used for each dilution followed by a 40 min dissociation. Chip surface was regenerated using pH 2.0 glycine between experiments.

ELISA

For the initial FLT1 blocking MAb screening, Nunc 96 well ELISA plates (ThermoFisher Scientific, 44-2404-21) were incubated with mouse FLT1-FC chimeric protein with His-tag (R&D systems, 471-F1-100). Plates were washed with 0.05% Tween 20/PBS, and blocked with 5% BSA (Fisher Scientific, BP1600-1)/PBS. After washing, diluted anti-FLT 1 antibodies were incubated. After washing, recombinant mouse PlGF2 (R&D systems, 465-PL-010/CF) was incubated. After washing, biotin-conjugated anti-PlGF2 antibody (R&Dsystems, BAF465) was added followed by a Streptavidin-HRP (R&D systems, DY998). For a colormetric detection, plates were developed with 3,3′,5,5′-Tetramethylbenzidine (TMB) Liquid Substrate (Sigma-

bioRxiv preprint doi: https://doi.org/10.1101/609735; this version posted April 15, 2019. The copyright holder for this preprint (which was not certified by peer review) is the author/funder. All rights reserved. No reuse allowed without permission.

Aldrich, T0440) and the reaction was stopped with 0.5M H_2SO_4. Specs were read at 450 nm on spectramax M5 plate reader (Molecular Devices). For VEGFA-FLT1 blocking assays, 96 wells ELISA plates were incubated with recombinant mouse VEGFA ($VEGF_{164}$, R&D systems, 493-MV-025/CF). After washing, anti-FLT 1 antibodies were incubated with mouse FLT1-FC chimeric protein with His-tag (R&D systems, 471-F1-100). After incubation the antibody-FLT1-FC complex was added to the VEGFA-coated plates. A biotin conjugated anti-His-tag antibody (Bio-Connect, NB100-63172) was added followed by a Streptavidin-HRP (R&D systems, DY998). For a colormetric detection, TMB was used as described above. For measurement of free sFlt1 and VEGFA in the serum. Animals were IV injected with 20 mg/kg body weight either isotype control IgG or the MAB0702 twice a weekly for four weeks beginning at 4 weeks of age. Blood was collected for biomaker analysis. Serum concentrations of sFLT1 and VEGFA were measured by ELSA kits following company recommended protocols (R&D systems, DY471 and DY493). For a colormetric detection, TMB was used as described above.

Microarray and RNA-seq analysis

Microarray analysis was performed using the Affymetrix Transcriptome Analysis Console (TAC). Samples in each experiment were RMA normalized and the expression was acquired using the Affeymetrix Expression analysis console with gene level expression. Heatmaps were generated in the Graphpad 7.1 (Prism). The code for generating each graph is listed in the following table, along with the link to the data in tabular format. All the data was obtained from NCBI GEO: Exercise, ALS, DMD, BMD, FSHD GSE3307, Early DMD GSE465, *mdx* GSE466, GRMD GSE69040, Satellite cells GSE15155. All arrays were normalized to their respective controls.

bioRxiv preprint doi: https://doi.org/10.1101/609735; this version posted April 15, 2019. The copyright holder for this preprint (which was not certified by peer review) is the author/funder. All rights reserved. No reuse allowed without permission.

Statistics

Statistics and graphs were calculated using Graphpad 7.1(Prism). Students t-test or ANOVA was used to compare two or more groups. Multiple comparison adjustment was performed with comparisons of 3 groups or more. * indicates $p<0.05$, ** indicates $p<0.01$, *** indicates $p<0.001$, *** indicates $p<0.0001$.

Author contributions

Designing research study- MV, JB, ZZ, AA. Conducting experiments- MV, YM, JE. Acquiring data- MV, YM. Analyzing data- MV, YM. Providing regents- DK, SJ. Writing manuscript- MV, AA. All the authors approved the final manuscript.

Acknowledgments

We would like to thank Jake Trask for a critical reading. This work was supported by NIHT32-GM008244 and NIHF30AR066454 to MV, and NIH R03, MDA and a research grant from Shire HGT, a member of the Takeda group of companies to AA.

Conflict of Interest

MV, AA, SJ and DK are listed as inventors on a patent for antibody mediated therapy for DMD. JB, ZZ, and SJ are employed by Shire HGT, a member of the Takeda group of companies and own stock in the company. AA was funded by Shire HGT, a member of the Takeda group of companies for antibody mediated therapy for DMD.

bioRxiv preprint doi: https://doi.org/10.1101/609735; this version posted April 15, 2019. The copyright holder for this preprint (which was not certified by peer review) is the author/funder. All rights reserved. No reuse allowed without permission.

bioRxiv preprint doi: https://doi.org/10.1101/609735; this version posted April 15, 2019. The copyright holder for this preprint (which was not certified by peer review) is the author/funder. All rights reserved. No reuse allowed without permission.

References

1. Verma M et al. Flt-1 haploinsufficiency ameliorates muscular dystrophy phenotype by developmentally increased vasculature in mdx mice.. *Hum. Mol. Genet.* 2010;19(21):4145–59.

2. Im WB et al. Differential expression of dystrophin isoforms in strains of mdx mice with different mutations. [Internet]. *Hum. Mol. Genet.* 1996;5(8):1149–53.

3. Miyatake M et al. Possible systemic smooth muscle layer dysfunction due to a deficiency of dystrophin in Duchenne muscular dystrophy. *J. Neurol. Sci.* 1989;93(1):11–17.

4. Loufrani L et al. Flow (shear stress)-induced endothelium-dependent dilation is altered in mice lacking the gene encoding for dystrophin [Internet]. *Circulation* 2001;103(6):864–870.

5. Ito K et al. Smooth muscle-specific dystrophin expression improves aberrant vasoregulation in mdx mice. *Hum. Mol. Genet.* 2006;15(14):2266–2275.

6. Coral-Vazquez R et al. Disruption of the sarcoglycan-sarcospan complex in vascular smooth muscle: a novel mechanism for cardiomyopathy and muscular dystrophy. *Cell* 1999;98(4):465–474.

7. Lai Y, Thomas G, Yue Y, Yang H. Dystrophins carrying spectrin-like repeats 16 and 17 anchor nNOS to the sarcolemma and enhance exercise performance in a mouse model of muscular [Internet]. *J. Clin. ...* 2009;119(3). doi:10.1172/JCI36612.624

8. Asai A et al. Primary role of functional ischemia, quantitative evidence for the two-hit mechanism, and phosphodiesterase-5 inhibitor therapy in mouse muscular dystrophy. *PLoS One* 2007;2(8):e806.

9. Adamo CM et al. Sildenafil reverses cardiac dysfunction in the mdx mouse model of Duchenne muscular dystrophy [Internet]. *Proc. Natl. Acad. Sci.* 2010;107(44):19079.

10. Nelson MD et al. PDE5 inhibition alleviates functional muscle ischemia in boys with

bioRxiv preprint doi: https://doi.org/10.1101/609735; this version posted April 15, 2019. The copyright holder for this preprint (which was not certified by peer review) is the author/funder. All rights reserved. No reuse allowed without permission.

Duchenne muscular dystrophy. [Internet]. *Neurology* 2014;82(23):2085–91.

11. Martin E a. et al. Tadalafil Alleviates Muscle Ischemia in Patients with Becker Muscular Dystrophy [Internet]. *Sci. Transl. Med.* 2012;4(162):162ra155-162ra155.

12. Matsakas A, Yadav V, Lorca S, Narkar V. Muscle ERRγ mitigates Duchenne muscular dystrophy via metabolic and angiogenic reprogramming. [Internet]. *FASEB J.* [published online ahead of print: June 18, 2013]; doi:10.1096/fj.13-228296

13. Latroche C et al. Structural and Functional Alterations of Skeletal Muscle Microvasculature in Dystrophin-Deficient mdx Mice [Internet]. *Am. J. Pathol.* 2015;(July):1–13.

14. Kendall RL, Thomas KA. *Inhibition of vascular endothelial cell growth factor activity by an endogenously encoded soluble receptor (endothelial ceils/mitogenic inhibitor/alternative transcription/angiogenesis)*. 1993:

15. Hayashi S, McMahon AP. Efficient recombination in diverse tissues by a tamoxifen-inducible form of Cre: a tool for temporally regulated gene activation/inactivation in the mouse. [Internet]. *Dev. Biol.* 2002;244(2):305–18.

16. Ho VC, Duan L-J, Cronin C, Liang BT, Fong G-H. Elevated vascular endothelial growth factor receptor-2 abundance contributes to increased angiogenesis in vascular endothelial growth factor receptor-1-deficient mice. [Internet]. *Circulation* 2012;126(6):741–52.

17. Seki T et al. Ablation of endothelial VEG FR1 improves metabolic dysfunction by inducing adipose tissue browning [Internet]. *J. Exp. Med.* 2018;215(1):1–16.

18. Waters RE, Rotevatn S, Li P, Annex BH, Yan Z. Voluntary running induces fiber type-specific angiogenesis in mouse skeletal muscle. [Internet]. *Am. J. Physiol. Cell Physiol.* 2004;287(5):C1342-8.

19. Webster C, Silberstein L, Hays AP, Blau HM. Fast muscle fibers are preferentially affected

bioRxiv preprint doi: https://doi.org/10.1101/609735; this version posted April 15, 2019. The copyright holder for this preprint (which was not certified by peer review) is the author/funder. All rights reserved. No reuse allowed without permission.

in Duchenne muscular dystrophy. *Cell* 1988;52(4):503–513.

20. Rafael JA. Dystrophin and utrophin influence fiber type composition and post-synaptic membrane structure [Internet]. *Hum. Mol. Genet.* 2000;9(9):1357–1367.

21. Call J a, Warren GL, Verma M, Lowe D a. Acute failure of action potential conduction in mdx muscle reveals new mechanism of contraction-induced force loss. [Internet]. *J. Physiol.* 2013;591(15):3765–76.

22. Robciuc MR et al. VEGFB/VEGFR1-Induced Expansion of Adipose Vasculature Counteracts Obesity and Related Metabolic Complications. *Cell Metab.* 2016;23(4):712–724.

23. Okabe K, Kobayashi S, Yamada T, Kurihara T, Tai-nagara I. Neurons Limit Angiogenesis by Titrating VEGF in Retina [Internet]. *Cell* 2014;159(3):584–596.

24. Goel AJ, Rieder MK, Arnold HH, Radice GL, Krauss RS. Niche Cadherins Control the Quiescence-to-Activation Transition in Muscle Stem Cells [Internet]. *Cell Rep.* 2017;21(8):2236–2250.

25. Kong J-S et al. Suppression of neovascularization and experimental arthritis by D-form of anti-flt-1 peptide conjugated with mini-PEG(TM). [Internet]. *Angiogenesis* 2011;14(4):431–42.

26. Liston DR, Davis M. Clinically relevant concentrations of anticancer drugs: A guide for nonclinical studies. *Clin. Cancer Res.* 2017;23(14):3489–3498.

27. Christinger HW, Fuh G, De Vos AM, Wiesmann C. The Crystal Structure of Placental Growth Factor in Complex with Domain 2 of Vascular Endothelial Growth Factor Receptor-1. *J. Biol. Chem.* 2004;279(11):10382–10388.

28. Lambrechts D et al. VEGF is a modifier of amyotrophic lateral sclerosis in mice and humans and protects motoneurons against ischemic death. [Internet]. *Nat. Genet.* 2003;34(4):383–94.

29. Poesen K et al. Novel Role for Vascular Endothelial Growth Factor (VEGF) Receptor-1 and

bioRxiv preprint doi: https://doi.org/10.1101/609735; this version posted April 15, 2019. The copyright holder for this preprint (which was not certified by peer review) is the author/funder. All rights reserved. No reuse allowed without permission.

Its Ligand VEGF-B in Motor Neuron Degeneration [Internet]. *J. Neurosci.* 2008;28(42):10451–10459.

30. Sawano a. et al. Flt-1, vascular endothelial growth factor receptor 1, is a novel cell surface marker for the lineage of monocyte-macrophages in humans [Internet]. *Blood* 2001;97(3):785–791.

31. Fong GH, Zhang L, Bryce DM, Peng J. Increased hemangioblast commitment, not vascular disorganization, is the primary defect in flt-1 knock-out mice. *Development* 1999;126(13):3015–3025.

32. Miquerol L, Langille BL, Nagy A. Embryonic development is disrupted by modest increases in vascular endothelial growth factor gene expression. [Internet]. *Development* 2000;127(18):3941–3946.

33. Logsdon E a, Finley SD, Popel AS, Mac Gabhann F. A systems biology view of blood vessel growth and remodelling. [Internet]. *J. Cell. Mol. Med.* 2014;18(8):1491–508.

34. Gabhann F Mac, Ji JW, Popel AS. Computational model of vascular endothelial growth factor spatial distribution in muscle and pro-angiogenic cell therapy. *PLoS Comput. Biol.* 2006;2(9):1107–1120.

35. Springer ML et al. Localized arteriole formation directly adjacent to the site of VEGF-induced angiogenesis in muscle. [Internet]. *Mol. Ther.* 2003;7(4):441–9.

36. Gianni-Barrera R et al. VEGF over-expression in skeletal muscle induces angiogenesis by intussusception rather than sprouting. [Internet]. *Angiogenesis* 2013;16(1):123–36.

37. Verma M et al. Muscle Satellite Cell Cross-Talk with a Vascular Niche Maintains Quiescence via VEGF and Notch Signaling. [Internet]. *Cell Stem Cell* 2018;23(4):530–543.e9.

38. Koch S, Claesson-Welsh L. Signal transduction by vascular endothelial growth factor

bioRxiv preprint doi: https://doi.org/10.1101/609735; this version posted April 15, 2019. The copyright holder for this preprint (which was not certified by peer review) is the author/funder. All rights reserved. No reuse allowed without permission.

receptors. [Internet]. *Cold Spring Harb. Perspect. Med.* 2012;2(7):a006502.

39. Dewerchin M, Carmeliet P. PlGF: A Multitasking Cytokine with Disease-Restricted Activity [Internet]. *Cold Spring Harb. Perspect. Med.* 2012;2(8):a011056–a011056.

40. Olofsson B et al. Vascular endothelial growth factor B, a novel growth factor for endothelial cells. [Internet]. *Proc. Natl. Acad. Sci. U. S. A.* 1996;93(6):2576–81.

41. Hagberg CE et al. Targeting VEGF-B as a novel treatment for insulin resistance and type 2 diabetes. *Nature* 2012;490(7420):426–430.

42. Li X et al. Reevaluation of the role of VEGF-B suggests a restricted role in the revascularization of the ischemic myocardium. *Arterioscler. Thromb. Vasc. Biol.* 2008;28(9):1614–1620.

43. Latroche C et al. Coupling between Myogenesis and Angiogenesis during Skeletal Muscle Regeneration Is Stimulated by Restorative Macrophages. *Stem Cell Reports* 2017;9. doi:10.1016/j.stemcr.2017.10.027

44. Christov C et al. Muscle satellite cells and endothelial cells: close neighbors and privileged partners. *Mol. Biol. Cell* 2007;18(4):1397–1409.

45. Von Haehling S, Anker SD, Saitoh M, Ebner N, Ishida J. Myostatin inhibitors as pharmacological treatment for muscle wasting and muscular dystrophy. *JCSM Clin. Reports* 2017;2(1):1–10.

46. Wallace B et al. Anti-sFlt-1 Therapy Preserves Lung Alveolar and Vascular Growth in Antenatal Models of BPD. [Internet]. *Am. J. Respir. Crit. Care Med.* 2017;8(3):1–63.

47. Danko I, Chapman V, Wolff JA. The frequency of revertants in mdx mouse genetic models for Duchenne muscular dystrophy [Internet]. *Pediatr. Res.* 1992;32(1):128–131.

48. Muzumdar MD, Tasic B, Miyamichi K, Li L, Luo L. A global double-fluorescent Cre

bioRxiv preprint doi: https://doi.org/10.1101/609735; this version posted April 15, 2019. The copyright holder for this preprint (which was not certified by peer review) is the author/funder. All rights reserved. No reuse allowed without permission.

reporter mouse. [Internet]. *Genesis* 2007;45(9):593–605.

49. Bae DG, Kim TD, Li G, Yoon WH, Chae CB. Anti-flt1 peptide, a vascular endothelial growth factor receptor 1-specific hexapeptide, inhibits tumor growth and metastasis. *Clin. Cancer Res.* 2005;11(7):2651–2661.

50. Aartsma-Rus A, van Putten M. Assessing Functional Performance in the Mdx Mouse Model [Internet]. *J. Vis. Exp.* [published online ahead of print: March 27, 2014];(85). doi:10.3791/51303

51. Fukada S et al. Genetic background affects properties of satellite cells and mdx phenotypes. [Internet]. *Am. J. Pathol.* 2010;176(5):2414–24.

52. Schindelin J et al. Fiji: an open-source platform for biological-image analysis. [Internet]. *Nat. Methods* 2012;9(7):676–82.

bioRxiv preprint doi: https://doi.org/10.1101/609735; this version posted April 15, 2019. The copyright holder for this preprint (which was not certified by peer review) is the author/funder. All rights reserved. No reuse allowed without permission.

Figures legends

Figure 1: Postnatal deletion of *Flt1* can increase capillary density in skeletal muscle.

A. Experimental scheme for assessing angiogenic response from conditional *Flt1* deletion.

B. Representative images of CD31-stained cryosections from the skeletal muscle from $Flt1^{+/+}$ and $Flt1^{\Delta/\Delta}$ mice. Scale bars indicate 100 µm.

C. Increase in capillary density is dependent on $CAG^{CreERTM}$ as well as tamoxifen in the $Flt1^{Loxp/Loxp}$ background.

D. Increase in capillary density is rapid and sustained following tamoxifen (TMX) induction in on $CAG^{CreERTM}$:$Flt1^{Loxp/Loxp}$ mice more than 6 months following induction.

Figure 2: Increased angiogenesis is accompanied by worsened muscle pathology in the *mdx:Flt1*$^{\Delta/\Delta}$ mice.

A. Capillary density is increased in *mdx:*$Flt1^{\Delta/\Delta}$ mice in the skeletal muscle.

B. Skeletal muscle perfusion is increased in the TA muscle in *mdx:*$Flt1^{\Delta/\Delta}$ mice.

C. Representative images of Evans blue dye (EBD) and Sirus red staining to measure fibrosis in diaphragm to measure acute damage.

D. *mdx:*$Flt1^{\Delta/\Delta}$ mice show no difference in acute damage as judged by EBD.

E. *mdx:*$Flt1^{\Delta/\Delta}$ mice show increased in fibrosis as evaluated by Sirus red staining.

F. *mdx:*$Flt1^{\Delta/\Delta}$ mice show no difference in the grip strength normalized to body weight.

Figure 3: Endothelial cell-specific conditional deletion of *Flt1* in *mdx:Cdh5-Flt1*$^{\Delta/\Delta}$ mice improve capillary density and muscle phenotype.

A. Experimental scheme for assessing angiogenic response from conditional *Flt1* deletion.

bioRxiv preprint doi: https://doi.org/10.1101/609735; this version posted April 15, 2019. The copyright holder for this preprint (which was not certified by peer review) is the author/funder. All rights reserved. No reuse allowed without permission.

B. Representative images of CD31 staining for capillary density, Sirus red staining to measure fibrosis and Evans blue dye (EBD) to measure acute damage in the diaphragm. Scale bars indicate 100 μm.

C. Endothelial cell specific conditional deletion of *Flt1* is sufficient to increase the capillary density in diaphragm.

D. Endothelial cell specific conditional deletion of *Flt1* is sufficient to increase skeletal muscle perfusion.

E. Acute damage as judged by EBD is reduced in *mdx:Cdh5-Flt1*$^{\Delta/\Delta}$ mouse muscle.

F. Fibrosis is reduced in *mdx:Cdh5-Flt1*$^{\Delta/\Delta}$ mouse muscle as evaluated by sirus red staining.

Figure 4: Endothelial cell-specific conditional deletion of *Flt1* in *mdx:Cdh5-Flt1*$^{\Delta/\Delta}$ mice improve muscle phenotype.

A. Representative images of HE staining of diaphragm. Scale bars indicate 100 μm.

B. Diaphragm muscle fiber turnover is reduced in *mdx:Cdh5-Flt1*$^{\Delta/\Delta}$ mouse muscle as evaluated by centrally located nuclei (CLN).

C. Distributions of mean fiber diameter in TA muscle of *mdx:Cdh5-Flt1*$^{\Delta/\Delta}$ mice were skewed toward the bigger fiber size compared with the control *mdx:Cdh5-Flt1*$^{\Delta/\Delta}$ mice.

D. Grip strength is improved in *mdx:Cdh5-Flt1*$^{\Delta/\Delta}$ mice.

Figure 5: Systemic anti-FLT1 peptide improves skeletal muscle pathology in *mdx* mice

bioRxiv preprint doi: https://doi.org/10.1101/609735; this version posted April 15, 2019. The copyright holder for this preprint (which was not certified by peer review) is the author/funder. All rights reserved. No reuse allowed without permission.

A. Experimental scheme for treatment of *mdx* mice with systemic treatment using anti-FLT1 peptide.

B. Representative images of (top) CD31, (middle) gross whole mount and cryosections for EBD, (bottom) Sirus red staining of diaphragm in *mdx* mice treated with anti-FLT1 peptide. Scale bars indicate 100 μm.

C. Anti-FLT1 peptide injection increases capillary density in the *mdx* mouse muscle at high dose.

D. Anti-FLT1 peptide injection decreases EBD+ area in the *mdx* mouse muscle at high dose.

E. Anti-FLT1 peptide injection decreases fibrotic area in the *mdx* mouse muscle at high dose.

F. Anti-FLT1 peptide injection is sufficient to increase skeletal muscle perfusion in *mdx* mice at high dose.

G. Grip strength is improved by anti-FLT1 peptide injection at high dose in *mdx* mice.

Figure 6: MAbs against FLT1 for the treatment of muscular dystrophy in the *mdx* mice.

A. Experimental scheme for systemic treatment of *mdx* mice with systemic injection of anti-FLT1 antibody.

B. Representative images of (top) CD31, (middle) EBD and (bottom) Sirius red staining of diaphragm in *mdx* mice treated with anti-FLT1 antibody. Scale bars indicate 100 μm.

C. Capillary destiny is increased in MAB0702 antibody treated mice but not EWC antibody in *mdx* mice compared with isotype control.

D. MAB0702 but not EWC injection is sufficient to increase skeletal muscle perfusion in *mdx* mice.

bioRxiv preprint doi: https://doi.org/10.1101/609735; this version posted April 15, 2019. The copyright holder for this preprint (which was not certified by peer review) is the author/funder. All rights reserved. No reuse allowed without permission.

E. EBD+ area is decreased in MAB0702 antibody treated mice but not EWC antibody in *mdx* mice compared with isotype control.

F. Fibrotic area is decreased in MAB0702 antibody treated mice but not EWC antibody in *mdx* mice compared with isotype control.

G. Calcification is decreased in MAB0702 antibody treated mice but not EWC antibody in *mdx* mice compared with isotype control.

Figure 7: MAbs against FLT1 for the treatment of muscular dystrophy in the *mdx* mice.

A. Representative images of HE staining of diaphragm in *mdx* mice treated with anti-FLT1 antibody. Scale bars indicate 100 μm.

B. Diaphragm muscle fiber turnover is reduced in MAB0702 treated *mdx* mouse muscle as evaluated by centrally located nuclei (CLN).

C. Distributions of mean fiber diameter in TA muscle of MAB0702 treated *mdx* mice were skewed toward the bigger fiber size compared with compared with isotype control.

D. Grip strength is improved in *mdx* mice treated with MAB0702 antibody compared with isotype control.

E. Treadmill running time and distance (F) are improved in *mdx* mice following MAB0702 antibody treatment.

Figure 8: VEGFA expression is decreased in patients with DMD.

A. *VEGFA* is compromised in both the dog (GRMD) and mouse (*mdx*) models of DMD compared with wild-type animals.

bioRxiv preprint doi: https://doi.org/10.1101/609735; this version posted April 15, 2019. The copyright holder for this preprint (which was not certified by peer review) is the author/funder. All rights reserved. No reuse allowed without permission.

B. Heatmap of VEGF ligand and receptor genes from microarrays from patients with neuromuscular diseases including early DMD (<age 3), late DMD, BMD, FSHD and ALS along with normal human muscle (NHM) and muscle following exercise.

C. RNA-seq from patients with DMD show reduced *VEGFA* expression in muscle biopsies.

D. Heatmap of genes upstream and downstream of *VEGFA* from microarray from patients with various neuromuscular diseases along with normal human muscle (NHM) and muscle following exercise.

Figure 1

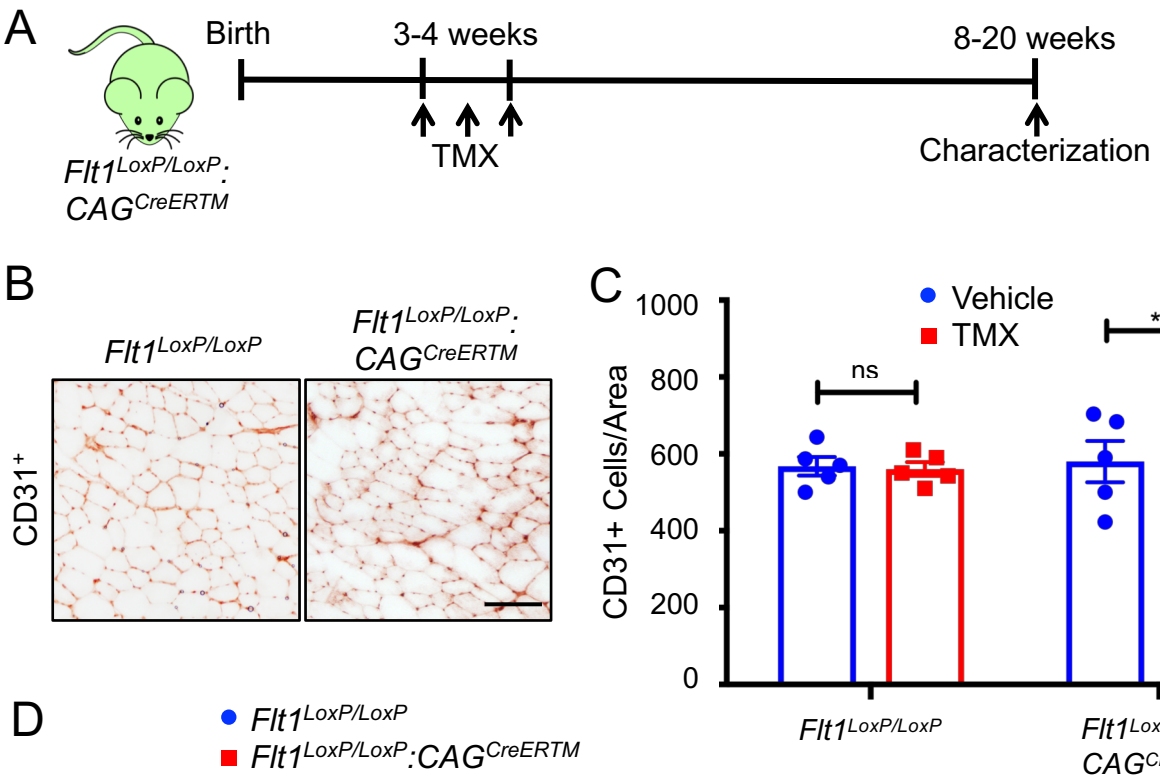
A
Birth
3-4 weeks
8-20 weeks
TMX
Characterization
Flt1LoxP/LoxP:
CAGCreERTM
B
Flt1LoxP/LoxP
Flt1LoxP/LoxP:
CAGCreERTM
CD31+
C
Vehicle
TMX
ns
*
CD31+ Cells/Area
1000
800
600
400
200
0
Flt1LoxP/LoxP
Flt1LoxP/LoxP:
CAGCreERTM
D
Flt1LoxP/LoxP
Flt1LoxP/LoxP:CAGCreERTM
CD31+ Cells/Area
1200
1000
800
600
400
200
0
*
ns
*
*
8
15
37
207
Days post TMX induction

Figure 2

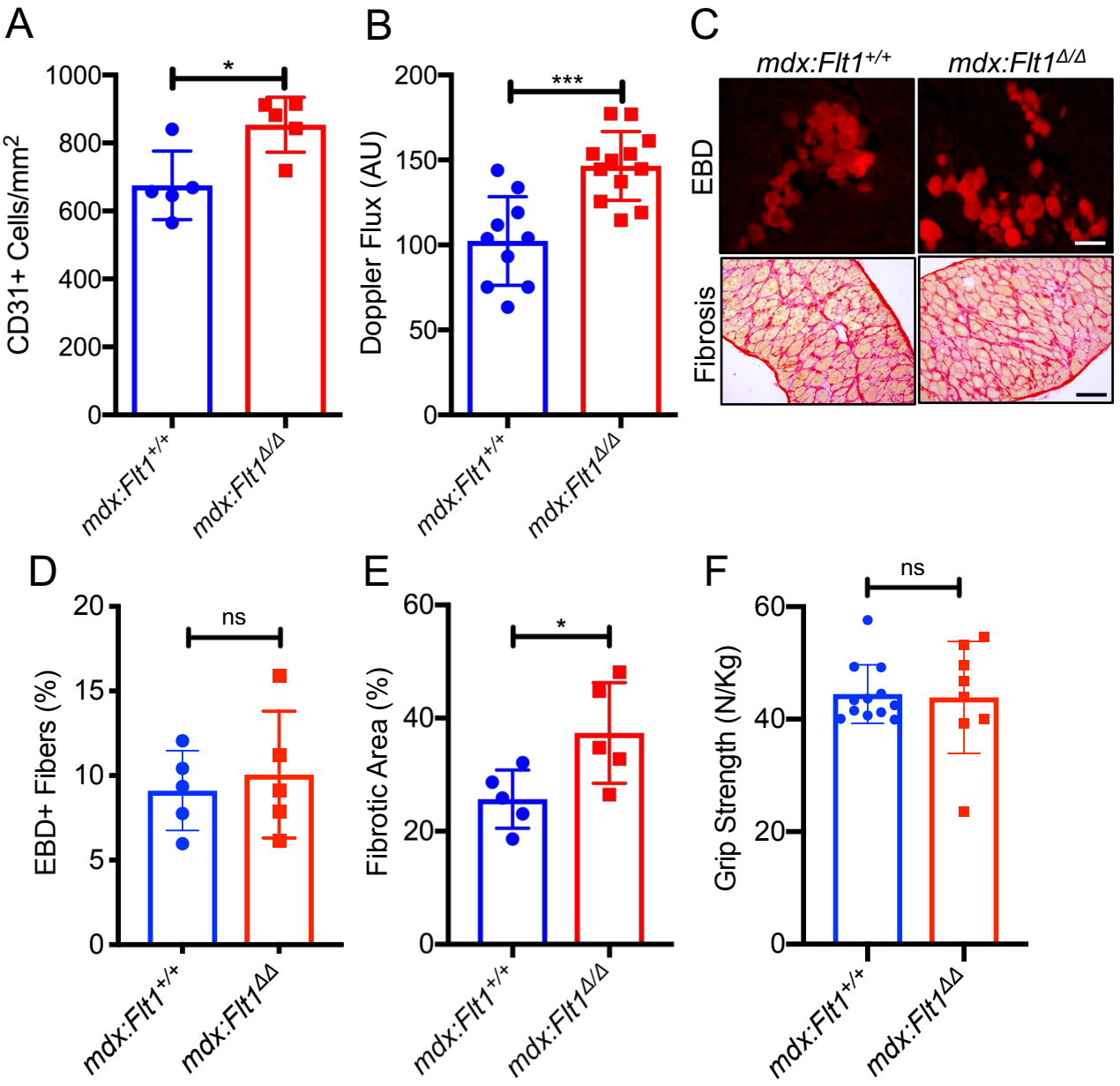
A
CD31+ Cells/mm2
1000
800
600
400
200
0
*
mdx:Flt1+/+
mdx:Flt1Δ/Δ
B
Doppler Flux (AU)
200
150
100
50
0
***
mdx:Flt1+/+
mdx:Flt1Δ/Δ
C
mdx:Flt1+/+
mdx:Flt1Δ/Δ
EBD
Fibrosis
D
EBD+ Fibers (%)
20
15
10
5
0
ns
mdx:Flt1+/+
mdx:Flt1ΔΔ
E
Fibrotic Area (%)
60
40
20
0
*
mdx:Flt1+/+
mdx:Flt1Δ/Δ
F
Grip Strength (N/Kg)
60
40
20
0
ns
mdx:Flt1+/+
mdx:Flt1ΔΔ

Figure 3

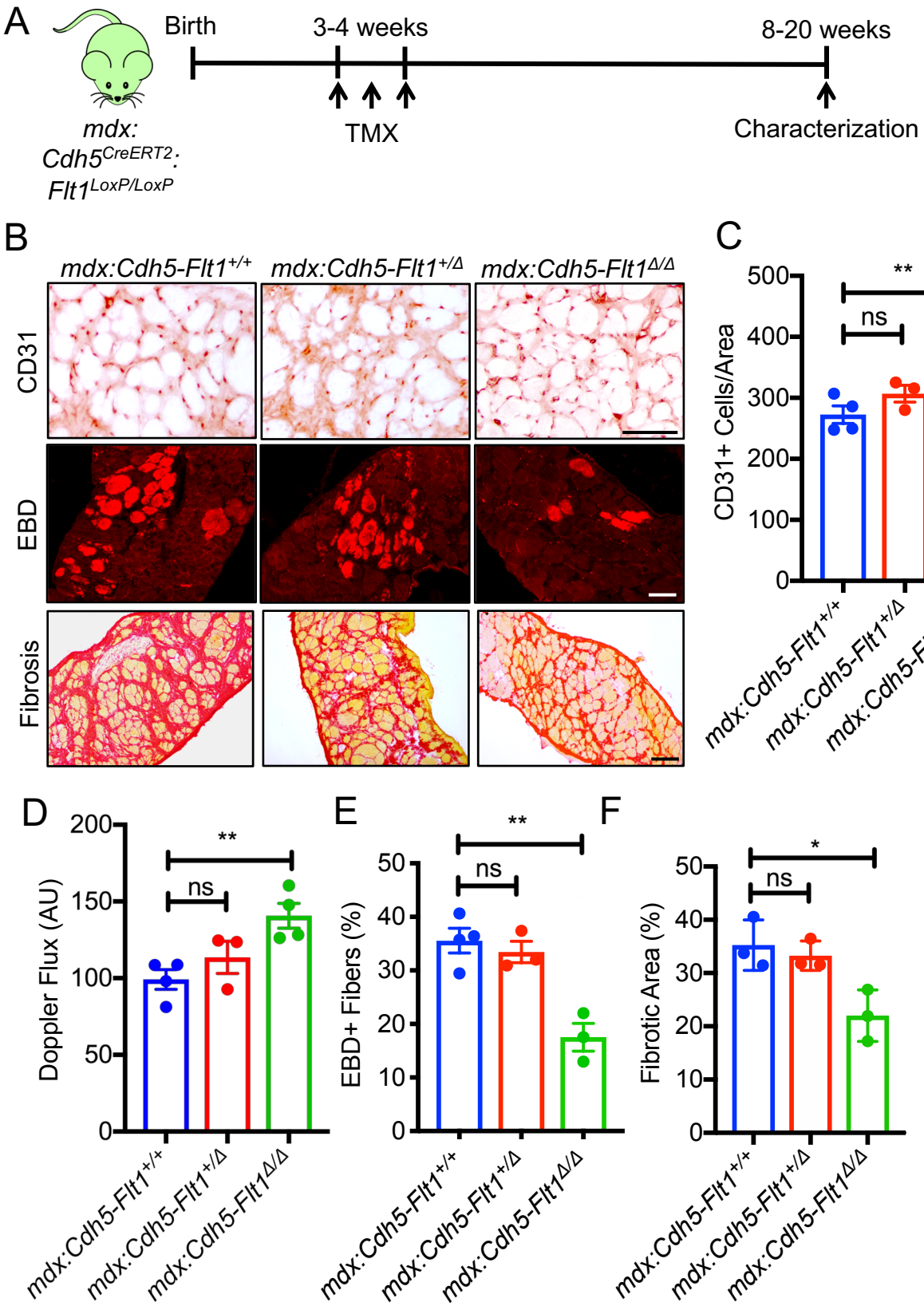
A
Birth
3-4 weeks
8-20 weeks
TMX
Characterization
mdx:
Cdh5CreERT2:
Flt1LoxP/LoxP
B
mdx:Cdh5-Flt1+/+
mdx:Cdh5-Flt1+/Δ
mdx:Cdh5-Flt1Δ/Δ
CD31
EBD
Fibrosis
C
CD31+ Cells/Area
500
400
300
200
100
0
**
ns
mdx:Cdh5-Flt1+/+
mdx:Cdh5-Flt1+/Δ
mdx:Cdh5-Flt1Δ/Δ
D
Doppler Flux (AU)
200
150
100
50
0
**
ns
E
EBD+ Fibers (%)
50
40
30
20
10
0
**
ns
F
Fibrotic Area (%)
50
40
30
20
10
0
*
ns

Figure 4

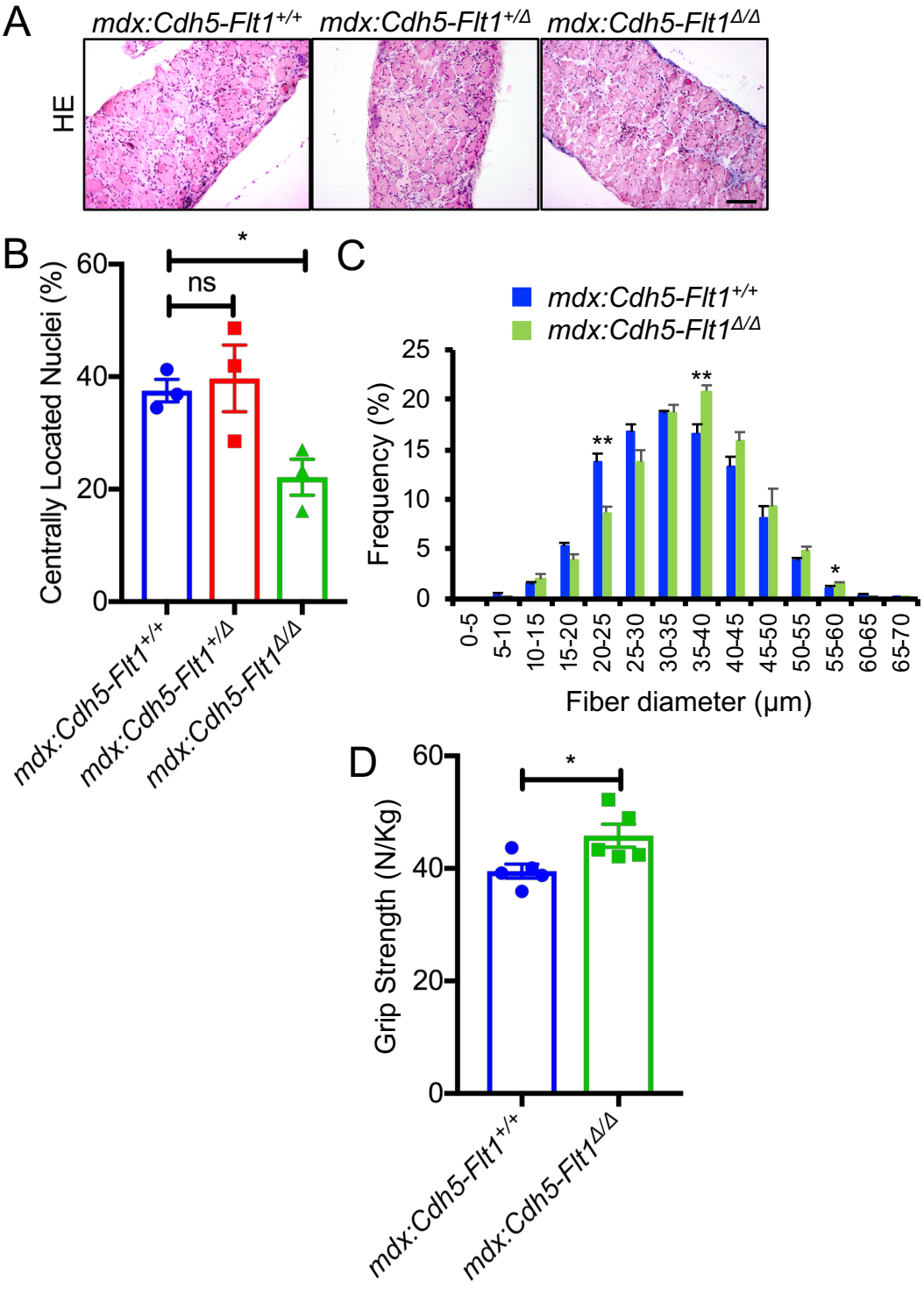
A
mdx:Cdh5-Flt1+/+
mdx:Cdh5-Flt1+/Δ
mdx:Cdh5-Flt1Δ/Δ
HE
B
Centrally Located Nuclei (%)
ns
*
mdx:Cdh5-Flt1+/+
mdx:Cdh5-Flt1+/Δ
mdx:Cdh5-Flt1Δ/Δ
C
mdx:Cdh5-Flt1+/+
mdx:Cdh5-Flt1Δ/Δ
Frequency (%)
Fiber diameter (μm)
0-5
5-10
10-15
15-20
20-25
25-30
30-35
35-40
40-45
45-50
50-55
55-60
60-65
65-70
D
Grip Strength (N/Kg)
mdx:Cdh5-Flt1+/+
mdx:Cdh5-Flt1Δ/Δ

Figure 5

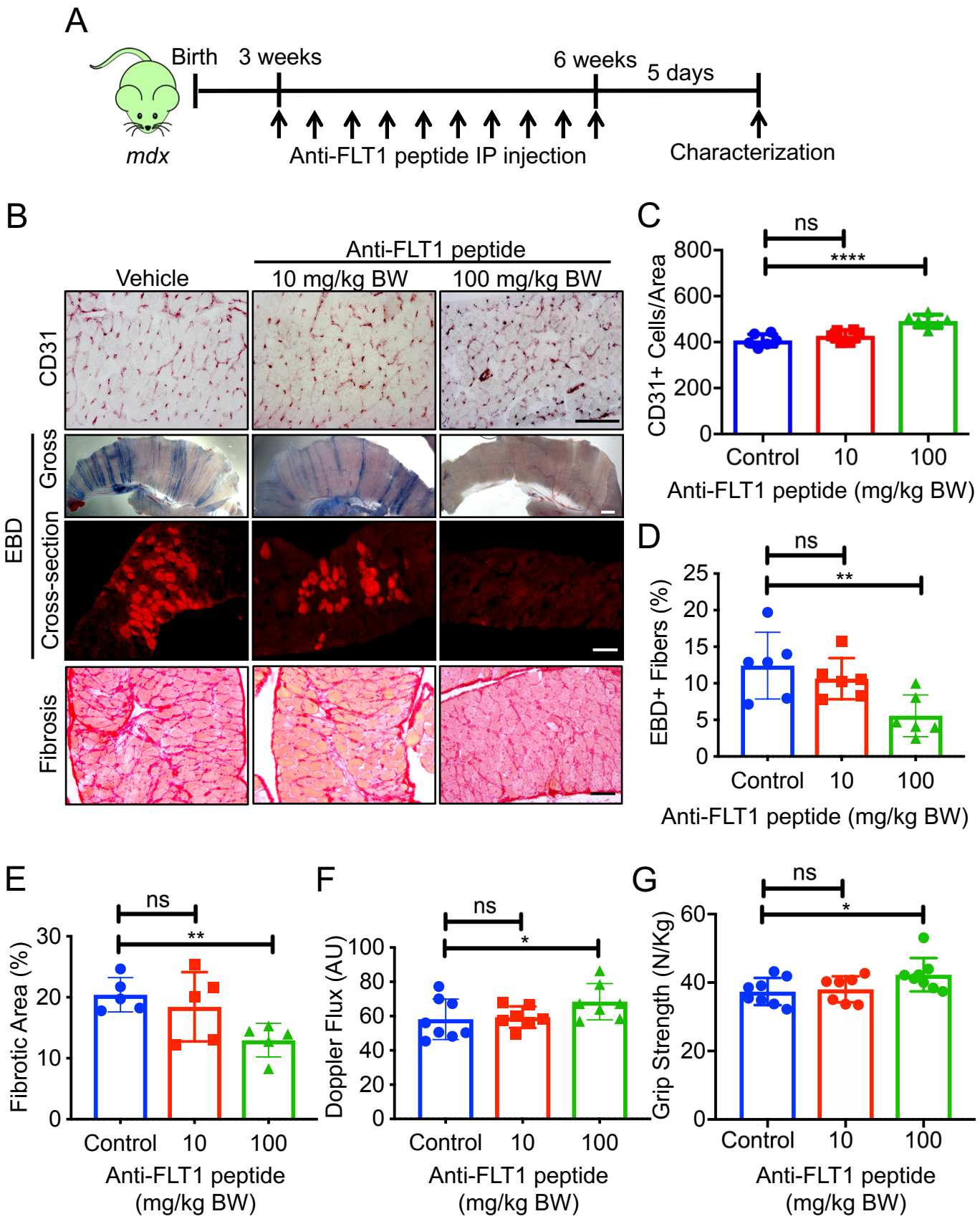
A
Birth
3 weeks
6 weeks
5 days
mdx
Anti-FLT1 peptide IP injection
Characterization
B
Anti-FLT1 peptide
Vehicle
10 mg/kg BW
100 mg/kg BW
CD31
EBD
Gross
Cross-section
Fibrosis
C
ns
****
CD31+ Cells/Area
800
600
400
200
0
Control
10
100
Anti-FLT1 peptide (mg/kg BW)
D
ns
**
EBD+ Fibers (%)
25
20
15
10
5
0
Control
10
100
Anti-FLT1 peptide (mg/kg BW)
E
ns
**
Fibrotic Area (%)
30
20
10
0
Control
10
100
Anti-FLT1 peptide
(mg/kg BW)
F
ns
*
Doppler Flux (AU)
100
80
60
40
20
0
Control
10
100
Anti-FLT1 peptide
(mg/kg BW)
G
ns
*
Grip Strength (N/Kg)
60
40
20
0
Control
10
100
Anti-FLT1 peptide
(mg/kg BW)

Figure 6

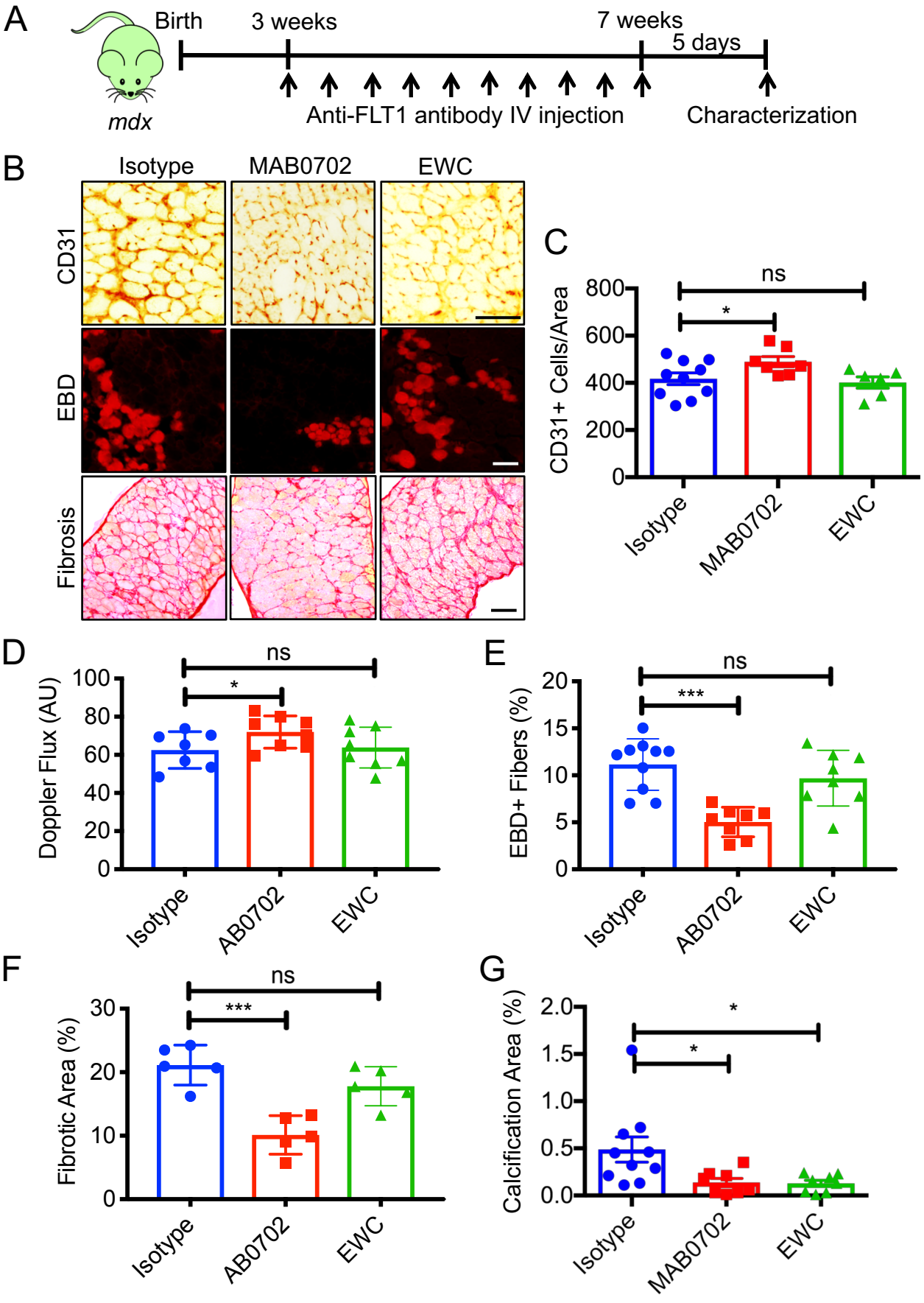
A
Birth
3 weeks
7 weeks
5 days
mdx
Anti-FLT1 antibody IV injection
Characterization
B
Isotype
MAB0702
EWC
CD31
EBD
Fibrosis
C
CD31+ Cells/Area
800
600
400
200
0
ns
*
Isotype
MAB0702
EWC
D
Doppler Flux (AU)
100
80
60
40
20
0
ns
*
Isotype
AB0702
EWC
E
EBD+ Fibers (%)
20
15
10
5
0
ns
***
Isotype
AB0702
EWC
F
Fibrotic Area (%)
30
20
10
0
ns
***
Isotype
AB0702
EWC
G
Calcification Area (%)
2.0
1.5
1.0
0.5
0.0
*
*
Isotype
MAB0702
EWC

Figure 7

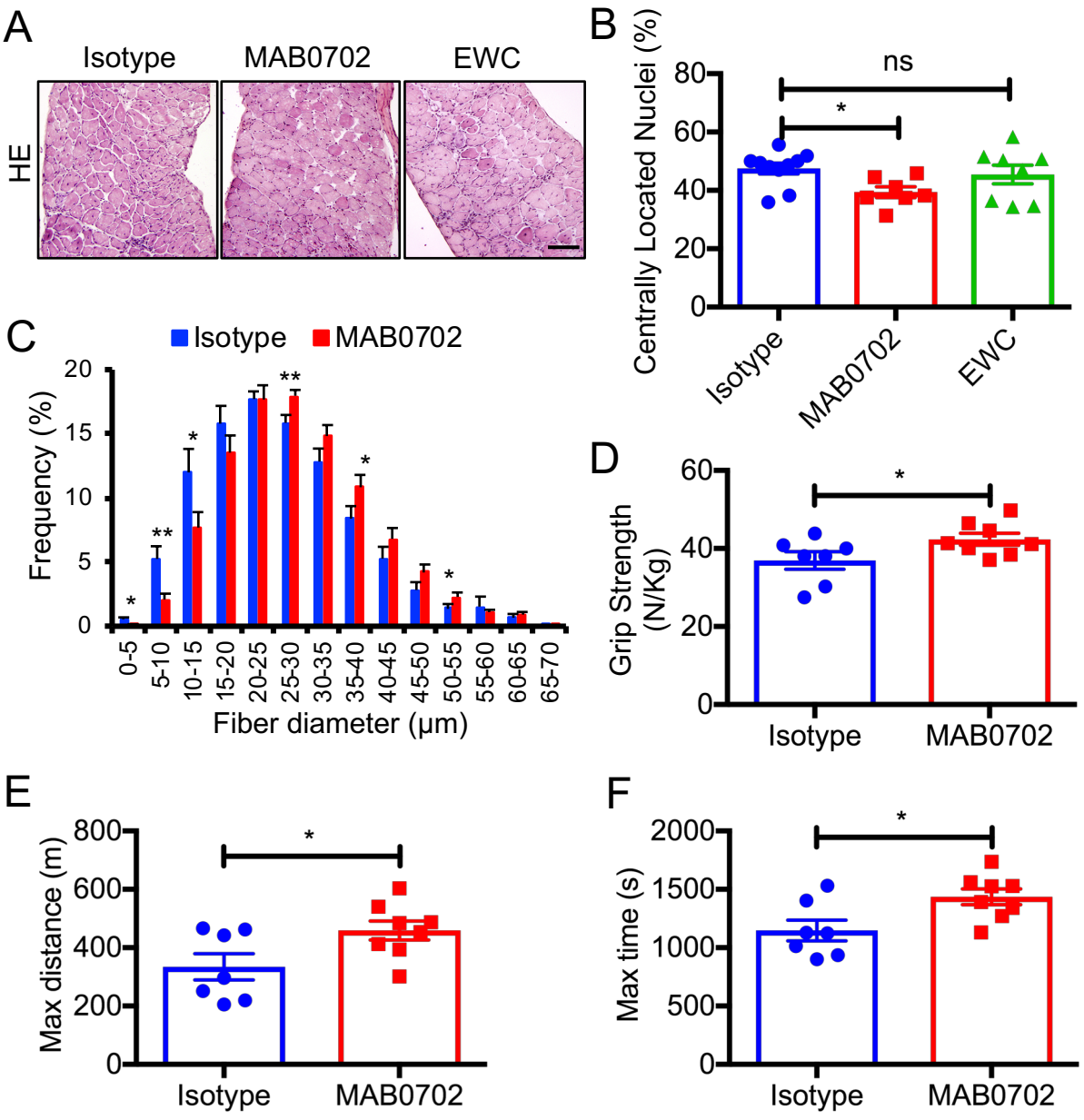
A
Isotype
MAB0702
EWC
HE
B
Centrally Located Nuclei (%)
ns
*
Isotype
MAB0702
EWC
C
Isotype
MAB0702
Frequency (%)
Fiber diameter (μm)
0-5
5-10
10-15
15-20
20-25
25-30
30-35
35-40
40-45
45-50
50-55
55-60
60-65
65-70
D
Grip Strength (N/Kg)
Isotype
MAB0702
E
Max distance (m)
Isotype
MAB0702
F
Max time (s)
Isotype
MAB0702

Figure 8

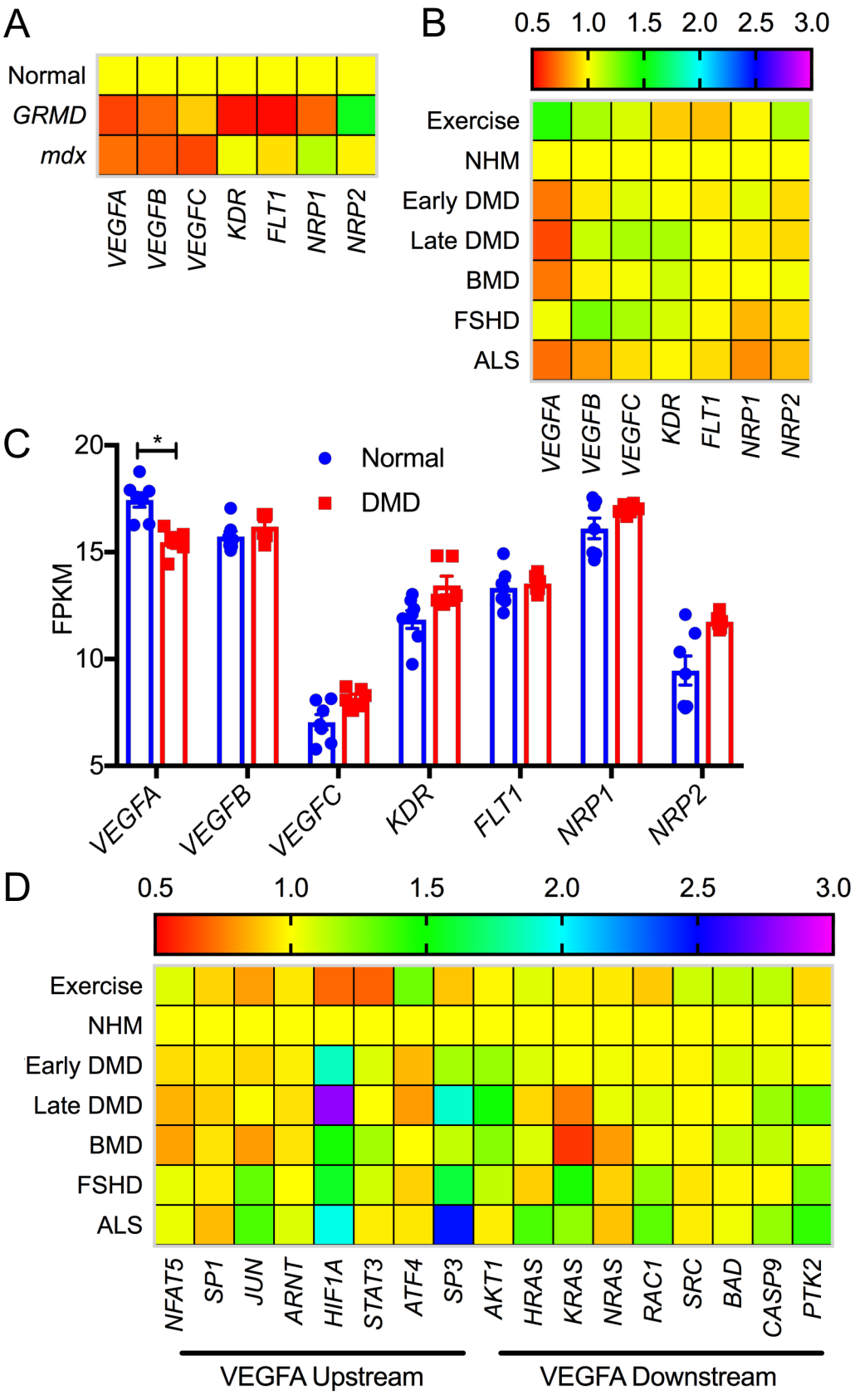
A
Normal
GRMD
mdx
VEGFA
VEGFB
VEGFC
KDR
FLT1
NRP1
NRP2
B
0.5 1.0 1.5 2.0 2.5 3.0
Exercise
NHM
Early DMD
Late DMD
BMD
FSHD
ALS
VEGFA
VEGFB
VEGFC
KDR
FLT1
NRP1
NRP2
C
FPKM
20
15
10
5
*
Normal
DMD
VEGFA
VEGFB
VEGFC
KDR
FLT1
NRP1
NRP2
D
0.5 1.0 1.5 2.0 2.5 3.0
Exercise
NHM
Early DMD
Late DMD
BMD
FSHD
ALS
NFAT5
SP1
JUN
ARNT
HIF1A
STAT3
ATF4
SP3
AKT1
HRAS
KRAS
NRAS
RAC1
SRC
BAD
CASP9
PTK2
VEGFA Upstream
VEGFA Downstream